Weierstraß-Institut
für Angewandte Analysis und Stochastik

Leibniz-Institut im Forschungsverbund Berlin e. V.

Preprint ISSN 2198-5855

Modeling hydrogen embrittlement for pricing degradation in gas pipelines

Zeina Amer[1], Ana Avdzhieva[2], Marcelo Bongarti[1], Pavel Dvurechensky[1], Patricio Farrell[1], Uwe Gotzes[3], Falk M. Hante[4], Attila Karsai[5], Stefan Kater[6], Manuel Landstorfer[1], Matthias Liero[1], Dirk Peschka[1], Luisa Plato[1], Klaus Spreckelsen[3], Johannes Taraz[7], Barbara Wagner[1]

submitted: June 16, 2025

[1] Weierstrass Institute
Mohrenstr. 39
10117 Berlin
Germany
E-Mail: dirk.peschka@wias-berlin.de

[2] Sofia University
Faculty of Mathematics and Informatics
1164 Sofia, 5 James Bourchier Blvd.
Bulgaria

[3] Open Grid Europe GmbH (OGE)
Kallenbergstr. 5
45141 Essen
Germany

[4] Humboldt-Universität zu Berlin
Institut für Mathematik
Unter den Linden 6
10099 Berlin
Germany

[5] Technische Universität Berlin
Institut für Mathematik
Straße des 17. Juni 136
10623 Berlin
Germany

[6] Albert-Ludwigs-Universität Freiburg
Abteilung für Angewandte Mathematik
Hermann-Herder-Str. 10
79104 Freiburg im Breisgau
Germany

[7] Delft University of Technology
Delft Institute of Applied Mathematics
Mekelweg 4, 2628 CD Delft
The Netherlands

No. 3201
Berlin 2025

2020 *Mathematics Subject Classification.* 35R02, 74A45, 74M10.

Key words and phrases. Hydrogen embrittlement, gas networks, fatigue damage.

Edited by
Weierstraß-Institut für Angewandte Analysis und Stochastik (WIAS)
Leibniz-Institut im Forschungsverbund Berlin e. V.
Mohrenstraße 39
10117 Berlin
Germany

Fax: +49 30 20372-303
E-Mail: preprint@wias-berlin.de
World Wide Web: http://www.wias-berlin.de/

Modeling hydrogen embrittlement for pricing degradation in gas pipelines

Zeina Amer, Ana Avdzhieva, Marcelo Bongarti, Pavel Dvurechensky, Patricio Farrell, Uwe Gotzes, Falk M. Hante, Attila Karsai, Stefan Kater, Manuel Landstorfer, Matthias Liero, Dirk Peschka, Luisa Plato, Klaus Spreckelsen, Johannes Taraz, Barbara Wagner

Abstract

This paper addresses aspects of the critical challenge of hydrogen embrittlement in the context of Germany's transition to a sustainable, hydrogen-inclusive energy system. As hydrogen infrastructure expands, estimating and pricing embrittlement become paramount due to safety, operational, and economic concerns. We present a twofold contribution: We discuss hydrogen embrittlement modeling using both continuum models and simplified approximations. Based on these models, we propose optimization-based pricing schemes for market makers, considering simplified cyclic loading and more complex digital twin models. Our approaches leverage widely-used subcritical crack growth models in steel pipelines, with parameters derived from experiments. The study highlights the challenges and potential solutions for incorporating hydrogen embrittlement into gas transportation planning and pricing, ultimately aiming to enhance the safety and economic viability of Germany's future energy infrastructure.

1 Introduction

As Germany transitions towards a sustainable and decarbonized energy system, hydrogen is emerging as a pivotal element in its future energy mix. The German National Hydrogen Strategy (Nationale Wasserstoffstrategie (NWS)) [Bun20], adopted in 2020, underscores the country's commitment to establishing hydrogen as a key pillar of its energy infrastructure, aiming to reduce greenhouse gas emissions and foster energy security. However, with the increased production, storage, and distribution of hydrogen, a critical challenge arises: *hydrogen embrittlement* that arises in existing steel pipelines when repurposing natural gas infrastructure.

Hydrogen embrittlement is a phenomenon in which certain metals become brittle and break due to hydrogen ingress, leading to deterioration in material properties (fatigue) and potential component failure [KP23]. This issue is particularly relevant for Germany's ongoing initiatives on building a national supply network through the upgrade and expansion of existing high-pressure gas networks. As such hydrogen infrastructure expands, so does the need for estimating and pricing hydrogen embrittlement, posing significant safety, operational, and economic concerns.

An important concern is that repeated pressure fluctuations, caused by line packing and other flexibilities in operational practices, impose cyclic loading on the pipeline, leading to metal fatigue. Over time, this can weaken the material and make it more susceptible to crack growth and material failure, especially in the presence of hydrogen. Suitable mathematical models for metal fatigue are usually based on fracture models that are formulated as nonlinear systems of partial differential equations [MHW10]. Several factors have been identified to affect hydrogen induced degradation of steel pipelines, e.g. (microstructural) material composition, frequency, gas pressure and purity [LDC$^+$22].

Currently, gas transportation planning is using typically stationary and capacity-based mathematical modelling and optimization of gas networks [HLM$^+$17, HS23]. Technical details on modelling and specialized mixed-integer programming techniques for solving the arising large-scale optimization problems can be found in [KHPS15]. The use of transient models for transportation planning is still rather limited due to the complex nature of the theoretically and computationally highly demanding models involving nonlinear partial differential equations.

DOI 10.20347/WIAS.PREPRINT.3201 Berlin 2025

However, mathematical modelling, simulation and optimization techniques have recently been advanced significantly in order to become applicable [HS24]. A direct application to avoiding or pricing embrittlement however remains highly challenging due to crack growth being a process on the scale of years rather then days.

In this context, our contribution is twofold: First, we discuss how hydrogen embrittlement can be modelled, using both continuum models and simplified models obtained by approximating relevant characteristics. Second, partly based on these results, we suggest optimization based pricing schemes for market makers. We consider setting the price using simplifying cyclic considerations within an economic model and discuss challenges for setting prices by using more detailed digital twin models. Both approaches build on widely-used model for subcritical crack growth in steel pipelines with parameters obtained from experiments. Therefore, the goal of this contribution is to outline a roadmap for realistic and mathematically tractable models of fatigue and hydrogen embrittlement in pipelines, which can serve as a basis for economic optimization models that account for pipeline ageing due to fatigue.

The paper is structured as follows. In Section 2, we study models for hydrogen embrittlement. We begin with a discussion on continuum models. Afterwards, we state a simplified model that can be used to estimate the lifetime of the pipe under cycling loading scenarios. In Section 3, we present a simplified economic model for pricing embrittlement on a single pipe and take first steps towards pricing models based on digital twins. Finally, in Section 4, we summarize our results and point towards future research directions.

2 Modeling hydrogen embrittlement

In this section, we introduce the phenomenology of hydrogen embrittlement and corresponding simplified fracture models and then we discuss an approximate lifetime function based on the current simplified mathematical model used by companies such as Open Grid Europe (OGE) to compute fatigue of pipelines filled with hydrogen. The basis of the simplified model is material data from the public report by the German Technical and Scientific Association for Gas and Water (DVGW) [SMS23]. In this model, the growth of cracks is computed via Paris' law $\frac{\mathrm{d}a}{\mathrm{d}N} = C(\Delta K)^m$ [PE63]. If the cracks become too deep or the stress induced by the cracks becomes too large, the pipe segment is in danger of leaking and has reached the end of its lifetime L. The model computes the change of crack depth $\frac{\mathrm{d}a}{\mathrm{d}N}$ and half crack length $\frac{dc}{\mathrm{d}N}$ during a certain number of cycles N of loading and unloading with a given pressure profile. In general, Paris' law (or the Paris–Erdogan equation) is an empirical system of ordinary differential equations (ODE) for crack growth

$$\frac{\mathrm{d}a}{\mathrm{d}N} = C_a(\Delta K_a)^m, \qquad \frac{\mathrm{d}c}{\mathrm{d}N} = C_c(\Delta K_c)^m, \tag{1}$$

where $C_i > 0$ and exponent $m \geq 2$ depend on the setup, material, and crack geometry, i.e. semielliptical surface cracks. The stress intensity factor K_i estimates the stress near the crack tip, with $\Delta K_i = K_{i,\max} - K_{i,\min}$ denoting the range of stress intensity during one cycle, see [NJR81].

2.1 Continuum models for hydrogen embrittlement

Hydrogen embrittlement is a phenomenon in materials science characterized by the degradation of mechanical properties in metals and alloys due to the diffusion of hydrogen into the crystal lattice of a material, leading to reduced ductility, increased brittleness, and a heightened susceptibility to fracture, even under relatively low applied stress levels. Recent discussion can be found in [AWL$^+$18, CMMP22, SMS23, HG20, MHW10, NBTB23, PZB$^+$19, SGAPJ21, WDM$^+$19, YSM22, ZÁB$^+$23]. As a result a material undergoes irreversible fatigue processes that induce and enhance crack growth, limiting the usefulness of the metal materials impacted by embrittlement under mechanical stress. Some of the main mechanisms that contribute to embrittlement are mentioned in Table 1.

Effect	Microscopic Mechanism
hydrogen pressure theory	Hydrogen atoms diffuse to and accumulate at defects, where they recombine into hydrogen molecules. This creates a high hydrogen gas pressure, which beyond a critical material stress leads to hydrogen-induced cracking.
HEDE	*Hydrogen-Enhanced DEcohesion:* Increasing hydrogen concentration reduces the cohesive forces (i.e. fracture toughness) through microscopic processes such as intergranular fracture.
HELP	*Hydrogen-Enhanced Localized Plasticity:* Higher hydrogen concentrations (by increased mobility and nucleation rate of dislocations) enhances plastic effects and therefore enhances crack propagation.

Table 1: Overview of primary mechanisms proposed for hydrogen embrittlement. Additionally, the mechanisms **NVC** (nanovoid coalescence), **HIPT** (hydrogen-induced phase transformation), and **HESIV** (hydrogen-enhanced strain-induced vacancies) are frequently discussed in the literature [LMZ+20]. All these effects intrinsically combine aspects of fracture, fatigue, and dislocation dynamics with chemomechanical coupling of hydrogen diffusion, where the microscopic origin of many thermodynamic phenomena for hydrogen embrittlement is still under debate.

Mathematical models for hydrogen embrittlement are coupled (continuum mechanical) descriptions of fracture that take, for example, the *elastic displacement* $u(t,x) \in \mathbb{R}^d$, the *fracture phase field* $\varphi(t,x) \in (0,1)$ and the *hydrogen concentration* $\psi(t,x) \in \mathbb{R}$ into consideration [YSM22, MWH10, CMMP22, HG20]. In many cases, to ensure good mathematical properties and thermodynamic consistency, such a model can be phrased in terms of a thermodynamic framework where, for isothermal systems, the free energy $\mathscr{F}$ decreases with time and this decrease can be guaranteed [MWH10]. A suitable (simplified) free energy for hydrogen embrittlement is

$$\mathscr{F}(u,\varphi,\psi) = \int_\Omega W(\psi,\nabla\psi,\varphi,\nabla\varphi,u,\nabla u)\mathrm{d}x \quad \text{with} \quad W = W_{\mathrm{mech}} + W_{\mathrm{frac}} + W_{\mathrm{H}_2},$$

with $W : \mathbb{R}\times\mathbb{R}^d\times\mathbb{R}\times\mathbb{R}^d\times\mathbb{R}^d\times\mathbb{R}^{d\times d} \to \mathbb{R}$, where W_{mech} contains all (elastic) mechanical contributions to the free energy, W_{frac} contains the energy for the fracture phase field that encodes the crack resistance and W_{H_2} contains the thermodynamical free energy of the hydrogen concentration. We consider the following decomposition of the total energy:

$$W_{\mathrm{mech}}(\psi,\varphi,u,\boldsymbol{F}) = \tfrac{\mu}{2}\,\varphi^2(1-\alpha\psi)\,|\boldsymbol{F}-\boldsymbol{F}_0(\psi)|^2 - f\cdot u, \tag{2a}$$

$$W_{\mathrm{frac}}(\psi,\varphi,\nabla\varphi) = G(\psi)\Big(\tfrac{\varepsilon}{2}|\nabla\varphi|^2 + \tfrac{1}{4\varepsilon}(1-\varphi)^2\Big), \tag{2b}$$

$$W_{\mathrm{H}_2}(\psi,\nabla\psi) = k_1\,\psi(\log\psi - 1) + k_2\,|\nabla\psi|^2, \tag{2c}$$

In the mechanical energy density (2a), the elastic modulus μ is multiplied by the degradation factor $(1-\alpha\psi)$,

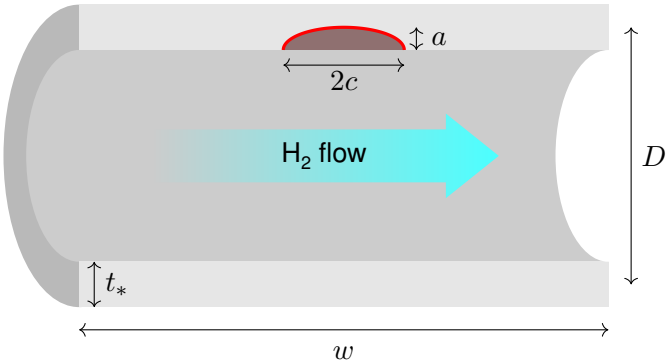

Figure 1: Sketch of a pipeline cross section with semielliptical surface crack (red) of **depth** a and **length** c for a pipe of diameter D and length w and thickness t_*; geometry adopted from [OFM25].

with $\alpha > 0$, and models a linearized hydrogen-induced softening of the material's elastic response (assuming $\alpha\psi < 1$). This effect is consistent with the HELP mechanism, wherein hydrogen facilitates dislocation motion by locally reducing resistance to deformation. We use the custom abbreviation $\boldsymbol{F} = \boldsymbol{I} + \nabla u$ for the deformation gradient. The function $\boldsymbol{F}_0$ describes the possible expansion and the generation of excess volumetric pressure due to the presence of hydrogen, i.e. the impact of hydrogen pressure theory. As common in phase-field models for fracture, the regularization parameter ε controls the width of the diffusive approximation of cracks. The function G in (2b) describes the dependence of the crack resistance on the hydrogen concentration. While for the moment we assume a constant toughness $G(\psi) = G_0$, the main impact of HEDE would be to decrease G with increasing ψ, i.e. $G(\psi) = G_0 - \beta\psi$. The parameter k_1 encodes the free energy of hydrogen in the lattice and drives diffusion, whereas k_2 is a mathematical regularization used to prevent (possibly artificial) high concentrations of hydrogen in regions of localised elastic stresses. The vector field $f : \Omega \to \mathbb{R}^d$ provides a given external mechanical load. For the elastic stress we introduce $\boldsymbol{\sigma} = \partial_{\boldsymbol{F}} W = \varphi^2(1-\alpha\psi)(\boldsymbol{F} - \boldsymbol{F}_0)$ and the chemical potential of the hydrogen $\eta = \partial_\psi W = -\frac{1}{2}\mu\varphi^2\alpha|\boldsymbol{F}|^2 - k_2\nabla^2\psi + k_1\log(\psi)$. We solve the following system of partial differential equations:

$$-\nabla\cdot\boldsymbol{\sigma} = f \qquad \text{static balance of mechanical stresses,} \tag{3a}$$

$$\eta = \lambda \qquad \text{static balance of chemical potential,} \tag{3b}$$

$$\partial_t\varphi = -M(\psi)[\partial_\varphi W - \nabla\partial_{\nabla\varphi} W] \qquad \text{dynamic fracture evolution,} \tag{3c}$$

together with conservation of mass $\int_\Omega \psi \,\mathrm{d}x = CV$ being enforced by a Lagrange multiplier $\lambda \in \mathbb{R}$ for a given average hydrogen concentration $C \in \mathbb{R}$ in the material of total volume $V = \int_\Omega 1 \,\mathrm{d}x$. Here, we describe a scenario where diffusion is much faster compared to the crack evolution caused by an external loading so that hydrogen embrittlement is always present.

This model neglects phenomena such as rate-independent plastic deformation, diffusion from the pressurised gas phase into the lattice, non-smooth dependence of W_{mech} on $\boldsymbol{F}$ and φ, crack healing, phase transitions and polycrystalline character of steel that are usually considered in literature [MHW10, TBW20]. The material parameters are artificial to exemplify embrittlement, i.e. $M(c) = 1$, $\mu = 10$, $\varepsilon = 0.02$, $G_0 = 1$, $\alpha = 0.2$, $k_1 = 1$, $k_2 = 0.1$, $f(x) = (0, 10x_2)$, $\boldsymbol{F}_0 = \boldsymbol{I}$, $C = 1$. The domain is $\Omega = ([-1,1]\times[0,6]) \setminus \omega$, where the convex hull $\omega = \mathrm{conv}\{(0,\pm 0.1),(0.2,0)\}$ serves as a cutout to nucleate a crack as shown in Figure 2.

One can make the following observations for this class of models: Assuming $\boldsymbol{F}_0 = \boldsymbol{I}$ and $k_2 = 0$, the stationary balance of the constant chemical potential can be solved for the concentration

$$\psi(t,x) = \psi_0 \exp\left(\tfrac{\mu}{2k_1}\varphi^2\alpha|\boldsymbol{F}(t,x) - \boldsymbol{I}|^2\right). \tag{4}$$

Here ψ_0 can be determined using the conservation of mass. This shows that one has a higher hydrogen concentration in regions of higher elastic stress, i.e. near a crack where the mechanical energy density is higher, see Figure 2. For $\alpha < 0$ hydrogen would be suppressed in regions of high elastic stresses. For $\alpha > 0$ the effect of hydrogen localisation near a crack depends on the magnitude of $\mu\alpha|\boldsymbol{F} - \boldsymbol{I}|^2/k_1 > 0$. The main effects that then enhance crack growth in the presence of hydrogen is the reduction of crack resistance with increasing hydrogen concentration encoded in $G(\psi)$ and the increase of crack mobility $M(\psi)$ with increasing hydrogen concentration encoded in $M(\psi)$. Additional effects due to $\boldsymbol{F}_0$ can also contribute. The local increase of hydrogen concentration in a stress field can be computed as in (4) under the made assumptions $k_2 = 0$ and constant $\boldsymbol{F}_0 = \mathbb{I}$. Larger $k_2 > 0$ would rather reduce variations of $\psi(t,x)$ and thereby reduce the hydrogen localisation near an advancing crack. Therefore, these combined effects give rise to hydrogen enhanced localised plasticity (HELP), hydrogen enhanced decohesion (HEDE) and via internal residual stresses and is visible theoretical models for advancing cracks, assuming hydrogen diffusion has enough time to reach a stationary state, see Figure 2. For faster crack evolution, a physical model would need to take into account a transient diffusion equation, e.g. standard diffusion would be of the form $\partial_t\psi - \nabla\cdot(m(\psi)\nabla\eta) = 0$ with mobility of diffusion m. A compelling argument for the dependence of embrittlement on loading frequency is provided, for example, by the authors of [YM17]. The recent experiments discussed before also strongly suggest the the crack advancement quantified via Paris' law is strongly frequency dependent and it is argued that embrittlement is more pronounced at sufficiently low frequencies, see [YM17, VCS12, LDC$^+$22].

A phase-field model as in (3) with validated material data might provide a framework that could quantify these effects. Works such as [YSM22] suggest that reasonable agreement with Paris' law can be achieved, but should be extended to explain such a frequency dependence. However, a more sophisticated model and and validated experiments are required to solve such a complex task.

The model above explains the phenomenology of hydrogen embrittlement and clearly shows, how diffusion adds a rate-dependent effect that competes with the time-scales of the other rate-dependent effects. However, for practical industrial applications usually simpler expressions for fatigue of steel pipelines are required.

2.2 Pipeline lifetime via Paris' law

The phase-field model (3) explains some aspects of hydrogen embrittlement and clearly shows how diffusion adds a rate-dependent effect that competes with the time scales of other rate-dependent and rate-independent effects. However, for practical industrial applications, simpler expressions for the fatigue of steel pipelines such as Paris' law [PE63] are usually required. In this section we derive an approximate formula for the lifetime of a specific pipe based on Paris' law in the form (1) and experimental data from the SyWeSt H2 study [SMS23]. This leads to a coupled ODE model, i.e. the *full model*, for which the details such as material parameters are described in the Appendix A.1 From the full model we derive an *approximation*, based on which we derive an

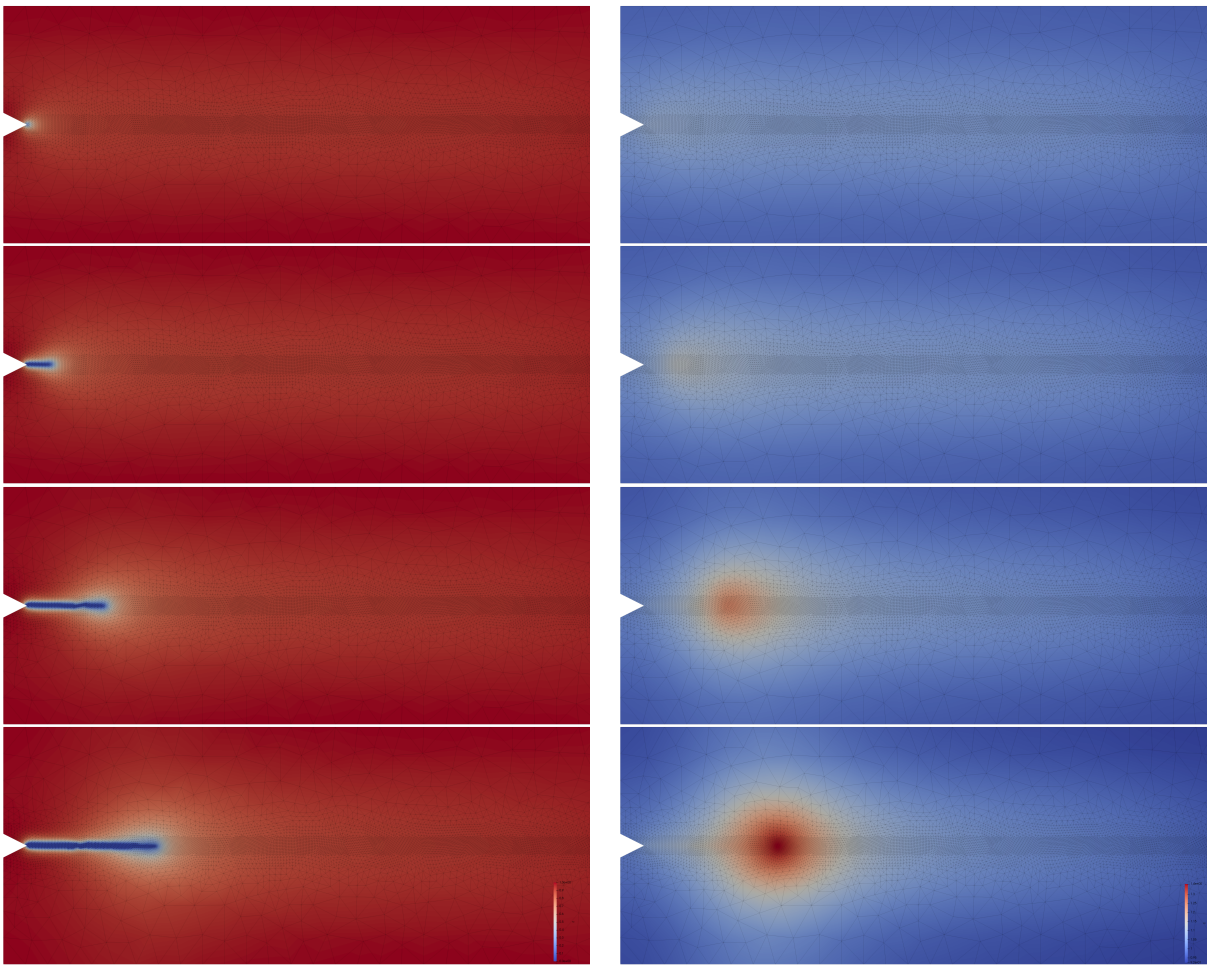

Figure 2: Solution of phase-field model for crack growth with stress induced diffusion (3) (left) showing the phase field φ, where the blue shaded area indicates a crack and (right) hydrogen concentration, where red indicates a higher hydrogen concentration and blue a lower concentration. Time increases from (top) to (bottom) with $t = \{0.14, 0.29, 0.35, 0.39\}$ for the accelerating crack. The locally refined computational mesh is shown in the background with dark lines.

expression for the pipeline lifetime. The approximation is based on the following three assumptions:

- constant crack length $c = c_0$, (A1)
- small stress intensity, i.e. $\Delta K \leq K_{\mathrm{crit}} := \left(3.6667 \cdot 10^{-6}\sqrt{p_{\mathrm{H_2}}/\mathrm{bar}}\right)^{-0.25}\,\mathrm{MPa\,m^{1/2}}$, (A2)
- $a \geq a_{\mathrm{crit}}$ as a failure criterion for end of lifetime. (A3)

Since we approximate $c = c_0$, only the evolution of the crack depth $a(N)$ remains. Furthermore, the assumption of $\Delta K \leq K_{\mathrm{crit}}$ leads to a closed form expression for $\frac{\mathrm{d}a}{\mathrm{d}N}$ without distinction of different regimes, e.g. small vs large stress. The third assumption (A3) means that each pipeline segment has a specific a_{crit}, independent of Δp and $\bar{p}$, such that if $a(N) \geq a_{\mathrm{crit}}$, the segment has reached the end of its service life.

Since, under these assumptions, the ODE is also separable, we do not explicitly have to solve for $a(N)$. To judge the quality of our approximation we can then numerically compute the coupled evolution of a and c in the original model and compare the results to our approximate formula. This is done in Section 2.2.1. We derive the following approximation for the crack depth a:

$$\begin{aligned}\frac{\mathrm{d}a}{\mathrm{d}N} &= \beta \cdot (1+3R)\Delta K^7\sqrt{\bar{p}} = \left(1+3\frac{\bar{p}-\Delta p}{\bar{p}}\right)\Delta p^7 f(a)\sqrt{\bar{p}} \\ &= \left(4-3\frac{\Delta p}{\bar{p}}\right)\Delta p^7\sqrt{\bar{p}}f(a) = g(\Delta p,\bar{p})f(a),\end{aligned} \tag{5}$$

with more mathematical details provided in (17) in Appendix A.1. Here, β is a constant and R is the load ratio $R = \frac{K_{\min}}{K_{\max}} = \frac{\bar{p}-\Delta p}{\bar{p}}$. From this model we derive the maximal number of cycles via

$$\begin{aligned}\frac{\mathrm{d}a}{f(a)} = g(\Delta p,\bar{p})\mathrm{d}N \quad &\Rightarrow \quad \int_{a_0}^{a(N)}\frac{\mathrm{d}a}{f(a)} = g(\Delta p,\bar{p})N \\ &\Rightarrow \quad \bar{C} = \int_{a_0}^{a_{\mathrm{crit}}}\frac{\mathrm{d}a}{f(a)} = g(\Delta p,\bar{p})N_{\mathrm{crit}}\end{aligned}$$

where the integral over a gives a constant $\bar{C}$ that only depends on pipe parameters and the crack parameters a_0 and a_{crit}. From this we can deduce the approximation of the lifetime

$$L = N_{\mathrm{crit}}T_{\mathrm{cycle}} = T_{\mathrm{cycle}}\frac{\bar{C}}{g(\Delta p,\bar{p})} \sim \frac{\sqrt{\bar{p}}}{(4\bar{p}-3\Delta p)\Delta p^7}. \tag{6}$$

where the transition from maximal cycle number N_{crit} to lifetime L requires the known cycle period T_{cycle}, which is assumed here to be $T_{\mathrm{cycle}} = 1\mathrm{h}$. The prefactor is a function of $a_0, a_{\mathrm{crit}}, c_0$ and the material parameters. In the following section we only compare the scaling behaviour of the lifetime, i.e. the approximation's prefactor is computed using the full model's numerical results. At this point, it is important to note that the experiments in the SyWeSt H2 study [SMS23] were conducted with a cycle period of $T_{\mathrm{cycle}} = 1\mathrm{s}$, whereas more realistic loading scenarios typically correspond to $T_{\mathrm{cycle}} = 1\mathrm{h}$ to $1\mathrm{d}$.

2.2.1 Comparison of the full model and approximation

In this section we compare the numerical solution of the full model for the lifetime $L = N_{\mathrm{crit}}T_{\mathrm{cycle}}$, which is based on a *failure criterion* to be met for the crack state after N_{crit} cycles following the evolution from (1), with further details provided in Appendix A.1, to the approximation of L given in (6). In the full model there are four different failure criteria, i.e. conditions that separately mark the end of lifetime for a pipeline. In addition to a critical crack depth, these employ critical stresses such as brittle fracture ratio $\mathrm{Kr}_a = \frac{Mf_wM_{ma}(\bar{p}+\bar{\sigma})}{K_{\mathrm{IC}}}\sqrt{\frac{\pi a}{1000}}$ and the plastic collapse ratio $\mathrm{Lr}_a = \frac{M\bar{\sigma}}{R_e}$ and the maximal stress intensity factor $K_{a,\max}$. Then, the *failure*

criterion (FC) is defined by the state (and critical cycle $N = N_{\mathrm{crit}}$), at which one of the following conditions is met:

$$a \geq a_{\mathrm{crit}}, \qquad K_{a,\max} \geq K_{a,\mathrm{crit}}, \qquad \mathrm{Kr}_a \geq \mathrm{Kr}_{a,\mathrm{crit}}, \qquad \mathrm{Lr_a} \geq \mathrm{Lr_{a,crit}}. \tag{FC}$$

where here $a_{\mathrm{crit}} = t_*$, $\mathrm{Kr}_{a,\mathrm{crit}} = (1 - 0.14\,\mathrm{Lr}_a^2)\left(0.3 + 0.7\exp(-0.65\,\mathrm{Lr}_a^6)\right)$, $K_{a,\mathrm{crit}} = K_{\mathrm{IC}}$ the plane-strain fracture toughness, and $\mathrm{Lr_{a,crit}} = \frac{1}{2R_e}(R_e + R_m)$ with yield strength R_e and tensile strength R_m. While $a \geq t_*$ is an obviously sufficient condition for pipe failure, empirically the other conditions in (FC) can even be more relevant in certain cases. This means that, contrary to our assumption for the approximate formula (6), the general failure criterion in the full model is thus not just a function of a but also of c and the specific stresses.

Parameter	**Value**	**Parameter**	**Value**
Wall thickness t_*	8 mm	Pipe length w	12 000 mm
Centre diameter D	608 mm	Fracture toughness K_{IC}	55 MPa$\sqrt{\mathrm{m}}$
Yield strength R_e	485 MPa	Ultimate tensile strength R_m	570 MPa

Table 2: Geometric and material parameters used in the pipeline model; cf. [SMS23].

In the following we will use the material parameters specified in Table 2 and relations from Appendix A.1, in particular with a pipe wall thickness $t_* = 8\,\mathrm{mm}$. In Figure 3 we show the lifetime as a function of $\bar{p}$ with constant Δp and as a function of Δp and constant $\bar{p}$ respectively. We compare the lifetime calculated by our approximation to the numerical results of the full model. We note that in all graphs, the curves agree very well for lifetimes > 1 year. For shorter lifetimes there is a significant disagreement. This goes hand in hand with a stronger disagreement for larger initial cracks (in length and in depth). The reason behind this larger disagreement is the assumption of small stress. One observes especially good agreement around $\Delta p = 30$ bar for constant maximal pressure below $\bar{p} = 80$ bar, whereas for larger $\bar{p}$ the approximation tends to overestimates the lifetime in comparison with the numerical result.

To assess the individual assumptions made in approximation of the model and the failure criteria (FC), we use an intermediate model that we solve numerically. This model makes the same simplifying assumptions (A1) and (A2) for Paris' law but uses the same failure criteria (FC) as the full model. To compare the full numerical and the intermediate model, the evolution of crack depth and crack length can be seen in Figure 4. Firstly, for smaller pressures in panel (a) and (b), the failure condition that is first satisfied is always $a \geq a_{\mathrm{crit}} = t_* = 8a_0$, whereas for larger pressures in panel (c) and (d) the failure condition is $\mathrm{Kr}_a \geq \mathrm{Kr}_{a,\mathrm{crit}}$ except for the intermediate model in panel (c) for smaller crack length. For smaller cycle numbers, where $c = c_0$ is well justified, the intermediate model is always a good approximation of the full model. However, in particular for shorter cracks this assumption (A1) seems to be violated and leads to rather strong deviations in N_{crit}. For longer cracks with $c_0 = 10\,\mathrm{mm}$, the assumption (A1) appears to be better justified throughout the simulation for $N \leq N_{\mathrm{crit}}$.

In Figure 5 the relative error between the full and the simplified numerical model of the lifetime is shown as a function of the initial crack depth a_0 and the initial half crack length c_0. It can be seen that the error is quite small for $c_0 > 7\,\mathrm{mm}$. The reason behind this is the neglected evolution of c (cf. Figure 4). It is relevant to point out that the lifetime function approximates the scaling behaviour of the numerical results quite well even for $c_0 = 5\,\mathrm{mm}$ (cf. Figure 3). Since Figure 5 is only concerned with comparing the lifetime calculated numerically from the two models, it does not judge the approximation of the scaling behaviour directly.

2.2.2 From cyclic loading to general time-dependent pressure profiles

While the perfectly periodic conditions are easily achievable in laboratory conditions, the question of course arises, how to use relations such as the Paris' law (1) for non-periodic pressure profiles. For energy produced by natural resources such as wind and solar energy, we cannot expect periodic pressure curves. Thus we have

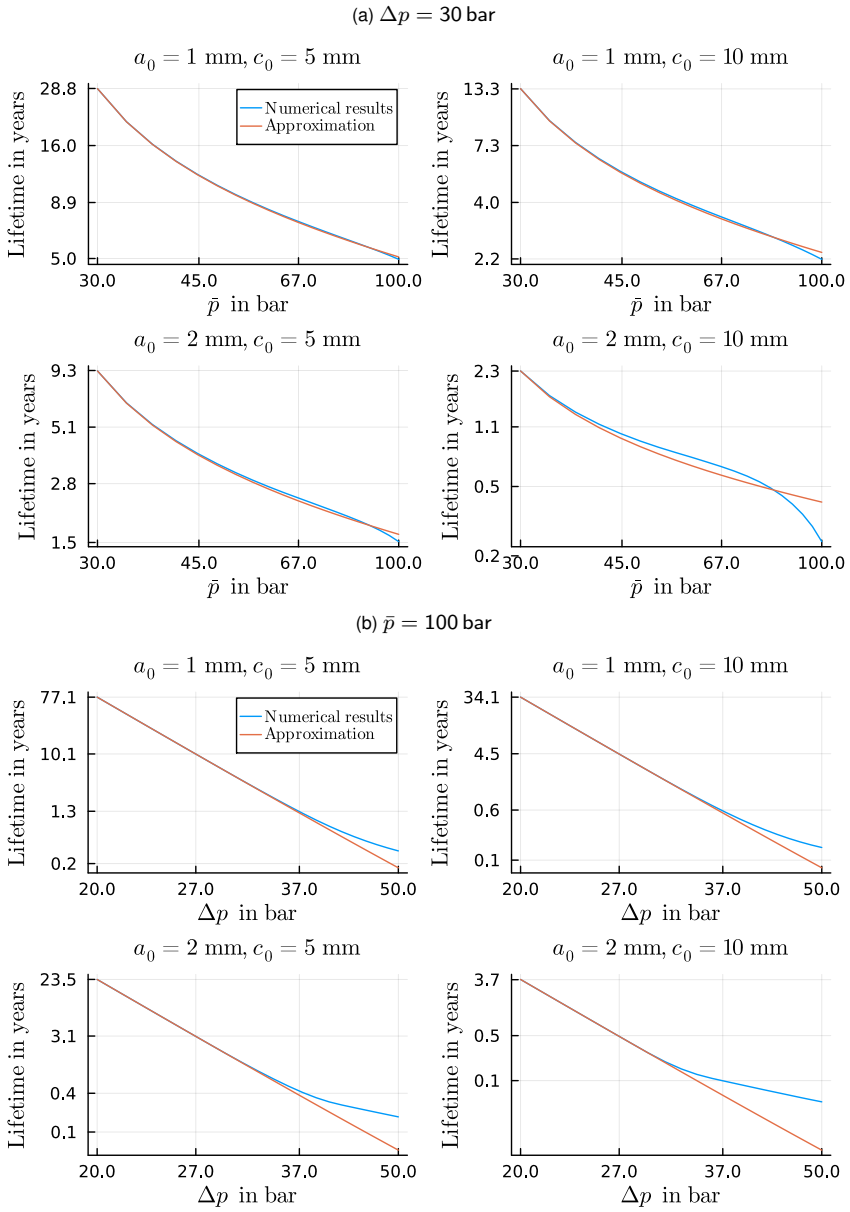

Figure 3: Comparison between the numerical results using the full model and our approximation of the lifetime function L for four different initial crack conditions. In the four top panels (a), $\Delta p = 30$ bar is kept constant. In the four bottom panels (b), $\bar{p} = 100$ bar is constant. Solutions are compared up to a scaling factor.

to give a new meaning to the pressure difference Δp and the maximal pressure $\bar{p}$. A strategy to identify $\bar{p}$ and Δp that is frequently used in this context is the so-called rainflow algorithm [DS82]. A main ingredient of this algorithm depicted in Figure 6, where a given stress or pressure profile (red, solid) is approximated by a piece-wise linear function (blue, dashed), connecting consecutively the pressure minima and maxima (circles).

We thus can identify tuples (t_i, p_i) for each turning point, that is local minimum or maximum of the linear approximation of the pressure curve, giving the pressure value p_i at time t_i for a given pressure curve. Note that this discretization of $p(t)$ does not at all lead to an equidistant discretization in time. However, one can now exploit the relation

$$\frac{\mathrm{d}a}{\mathrm{d}N} = f(a, c; \bar{p}, \Delta p, \alpha),$$

by using the rainflow-inspired discretization (t_i, p_i). We take the pressure difference to be $\Delta p_{i+1} = p_{i+1} - p_i$ and the maximal pressure $\bar{p}_{i+1}$ to be $\bar{p}_{i+1} = \max(p_i, p_{i+1})$. Since the distance from one turning point t_i to

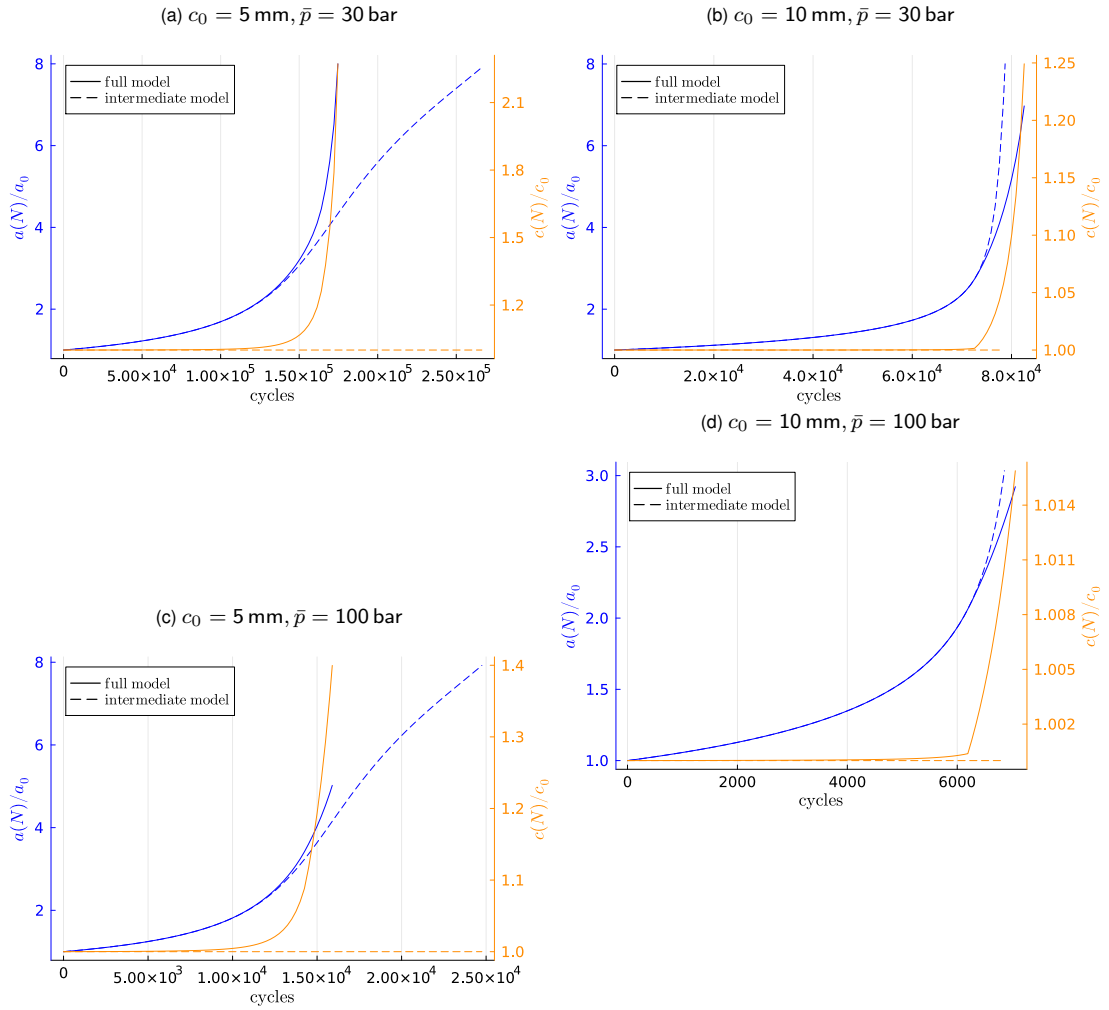

Figure 4: Comparison of numerical solutions of the full model (solid lines) and the intermediate model (dashed lines) for different initial crack length c_0 and pressure $\bar{p}$ as a function of cycles for $N \leq N_{\text{crit}}$. Solutions end at the cycle where one of the failure criteria (FC) is met. The other parameters are $a_0 = 1$ mm and $\Delta p = 35$ bar.

the next t_{i+1} is only half a cycle, we approximate

$$\frac{\mathrm{d}a}{\mathrm{d}N} \approx \frac{a_{i+1} - a_i}{2}.$$

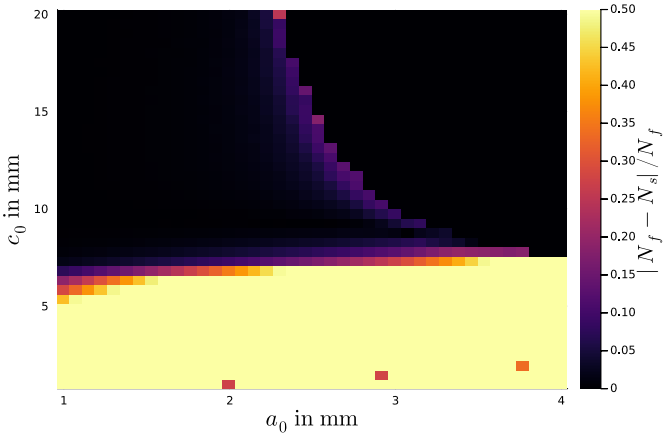

Figure 5: The relative error between the lifetime (or cycles) calculated numerically using the full model N_f and the simplified numerical model N_s is shown as a heatmap for different values of a_0 and c_0. All calculations are done with $\Delta p = 30$ bar, $\bar{p} = 100$ bar. The relative error is capped to 0.5, i.e. the colour actually shows $\min\{0.5, |N_f - N_s|/N_f\}$.

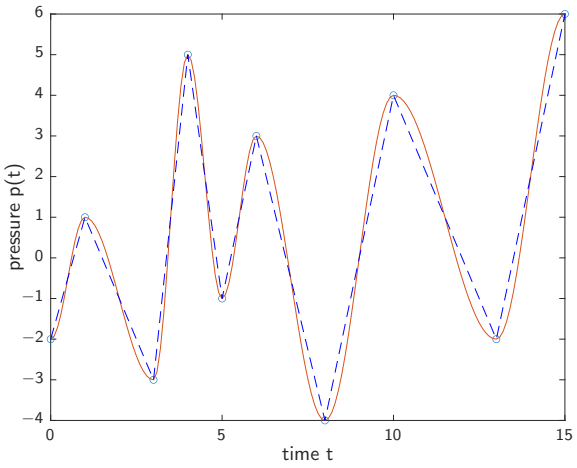

Figure 6: Pressure profile $p(t)$ and piece-wise linear approximation by the rainflow algorithm.

Putting this together, one can approximate the crack depth after one half-cycle by

$$a_{i+1} = a_i + 2f(a_i, c_i, \bar{p}_{i+1}, \Delta p_{i+1}, \alpha).$$

A similar scheme can be constructed for the crack length c. We strongly emphasise here that the actual time t_i does not occur in the discrete evolution equation. This originates from the Paris' law, which only counts how often the stress or pressure is changed, but not how long it took to achieve this pressure change. This is a crucial assumption of the model developed in SyWest H2 [SMS23]. Further extensions of Paris' Law, which can handle truly time varying pressure profiles also taking into account the length of loading cycles and not only the number of cycles were discussed in Section 2.1.

2.2.3 Limitations of Paris' law

Paris' law is well established and the basis for most industrial applications. Because of its simplicity it is extensively used in fatigue crack growth analysis. A good fit to experimental data can often be achieved for a wide range of materials and loading regimes. However, it does have some important limitations and experimental data can often deviate from Paris' law for a range of reasons. For example, Paris' law is valid only for sufficiently long cracks and not during early or late-stage propagation. In addition, deviations can also be seen for example as the load stress varies. Paris' law has thus been extended and modified in many ways over the last decades to account for the discrepancies with the aim to incorporate additional physics.

Crack growth laws:

$$\begin{aligned}
\text{Paris \& Erdogan (1963) [PE63]}: &\quad \frac{\mathrm{d}a}{\mathrm{d}N} = C\Delta K^n (K_{\max})^m \\
\text{Forman, Kearny, Engle (1967) [FKE67]}: &\quad \frac{\mathrm{d}a}{\mathrm{d}N} = f(\Delta K, R, K_c) \\
\text{Tomkins (1968) [Tom68]}: &\quad \frac{\mathrm{d}a}{\mathrm{d}N} = f(\Delta CTOD) \\
\text{Wolf et al. (1970) [Wol70]}: &\quad \frac{\mathrm{d}a}{\mathrm{d}N} = C(\Delta K_{\text{eff}})^n \\
\text{Walker (1970) [Wal70]}: &\quad \frac{\mathrm{d}a}{\mathrm{d}N} = f(\Delta K, R) \\
\text{Dowling \& Begley (1976) [DB76]}: &\quad \frac{\mathrm{d}a}{\mathrm{d}N} = C(\Delta J_{\text{eff}})^n \\
\text{Ogura et al. (1985) [OMN85]}: &\quad \frac{\mathrm{d}a}{\mathrm{d}N} = f(W_{\text{eff}})
\end{aligned}$$

For an overview see [NJ98]. Even though Paris' Law delivers a good fit under certain parameter regimes, these growth laws are typically still at the heart of empirical laws. In particular the ability to capture the frequency dependence of crack propagation under the presence of hydrogen is rather limited. In fact, the problem of fatigue with hydrogen embrittlement cannot be adequately represented as shown in Vergani [VCS12]. However, while experiments have shown that crack growth with hydrogen embrittlement is frequency dependent, Paris' law formulated in cycles is frequency independent [PE63]. Paris' law is only valid for high frequency loading [PCCC06] – for lower frequencies the growth rate is markedly higher. A simplified explanation of this effect is: Hydrogen enhances growth rate – thus higher than Paris' law, but it requires sufficient time for diffused hydrogen to concentrate and soften the tip – so this only affects growth for low frequencies. This suggests modifications required for lower frequencies: either based off Paris' law (e.g. other curves on graph) or to develop continuum models based on underlying physical mechanisms.

3 Pricing embrittlement

Current gas transportation planning predominantly relies on stationary and capacity-based mathematical modelling and optimization. The effects of pipeline degradation is not accounted for in market design as well as in the operational planning. In this section, we address these challenges using two approaches. First, we propose optimization-based pricing schemes for market makers. We consider setting prices using simplified cyclic loading considerations within an economic model. Then we discuss the challenges associated with using more detailed digital twin models.

3.1 An economic model for pricing embrittlement

We start by simplifying the gas network considerably. Our model is concerned with a single pipe model and focuses on three aspects of interest: a *capacity* product, a *flexibility* product, and the lifetime of the pipe. Currently, the focus is typically on a capacity product. Capacity is the amount C, for which customers have the right to input (extract) the amounts $0 \leq X_{\text{in/out}} \leq C_{\text{in/out}}$ of gas to (from) the pipe over the time horizon $[0, \tau]$. They may use the entire booked capacity or only parts of it. Mathematically, this means that $X_{\text{in/out}}$ are defined as

$$X_{\text{in}} = \int_0^\tau q_{\text{in}} \,\mathrm{d}t \leq C_{\text{in}}, \qquad X_{\text{out}} = \int_0^\tau q_{\text{out}} \,\mathrm{d}t \leq C_{\text{out}},$$

where q_{in} and q_{out} are the input and output mass flows, and C_{in} and C_{out} are the input and output capacities, respectively. Moreover, we assume that the customer can buy flexibility over the time horizon $[0, \tau]$, which can

be described as the right to inject more (or less) gas than the contracted amount. In that case, we can define the flexibility quota as a number F such that

$$|X_{\text{out}} - X_{\text{in}}| = \left| \int_0^\tau q_{\text{out}} \, \mathrm{d}t - \int_0^\tau q_{\text{in}} \, \mathrm{d}t \right| \leq F. \tag{7}$$

This definition of flexibility implicitly assumes that the customer has control over both the in- and outflow of the pipe. With infinite flexibility, the customers would use the pipe as a temporary storage medium, potentially reducing the lifetime of the pipe. As this causes monetary disadvantages for network operators, the flexibility will need to be priced accordingly. Our model tries to capture this pricing problem by proposing an economic model based on pipeline life time.

In the following, we denote the maximal pressure at which we operate the pipe by $\overline{p}$, the minimal pressure at which we operate the pipe by $\underline{p}$, and the maximal pressure fluctuation by Δp. Furthermore, we denote the price for capacity by $M_C(\overline{p})$, the price for flexibility by $M_F(\Delta p)$, the lifetime of the pipe by $L(\overline{p}, \Delta p)$, and the monetary function $M(M_C, M_F)$. The functions M_C, M_F and M are assumed to be increasing in their respective arguments, and the function L is assumed to be decreasing with respect to both arguments.

We want to maximize revenue from selling capacity and flexibility, guaranteeing that the pipe will last a minimum life time of T years. The maximal pressure $\overline{p}$ cannot exceed a natural limit P. With the quantities α and β for the prices for the capacity and flexibility provided during one year, we arrive at the maximization problem

$$\left.\begin{aligned} &\max_{\Delta p, \overline{p}} \; T(\alpha M_C + \beta M_F) \\ &\text{subject to} \\ &L(\overline{p}, \Delta p) \geq T, \\ &0 \leq \overline{p} \leq P, \\ &\Delta p \leq \overline{p}. \end{aligned}\right\} \tag{8}$$

As a starting point, we make the following simple assumptions for the prices for capacity and flexibility. We price the capacity and flexibility in units of euros as

$$M_C(\overline{p}) = a\overline{p} + b, \tag{9}$$
$$M_F(\Delta p) = d\Delta p + e \tag{10}$$

and consider the total monetary function

$$M(M_C, M_F) = \alpha M_C + \beta M_F \tag{11}$$

for some positive constants α and β. We point out that this choice of M_F is directly linked to the definition of flexibility in (7), assuming that the maximal change in pressure Δp and the maximal change in mass flow Δq are related. Additionally, we start by considering a simple life time function of the pipe given by

$$L(\overline{p}, \Delta p) = \frac{1}{\Delta p^\kappa} \frac{1}{\overline{p}^\lambda}. \tag{12}$$

Later, we will consider a more realistic life time function. For these choices, the solution to the optimization problem (8) can be obtained using a geometric argument. We distinguish two cases:

- If $\alpha a \geq \beta d$, then the optimal solution is the right point $\bar{p} = P$, $L(\overline{p}, \Delta p) = T$ in Figure 7, which implies $\Delta p = \frac{1}{(TP^\lambda)^{1/\kappa}}$.
- If $\alpha a < \beta d$, then the optimal solution is the left point $\bar{p} = \delta p$, $L(\overline{p}, \Delta p) = T$ in Figure 7, which implies $\bar{p} = \Delta p = \frac{1}{T^{1/(\kappa+\lambda)}}$.

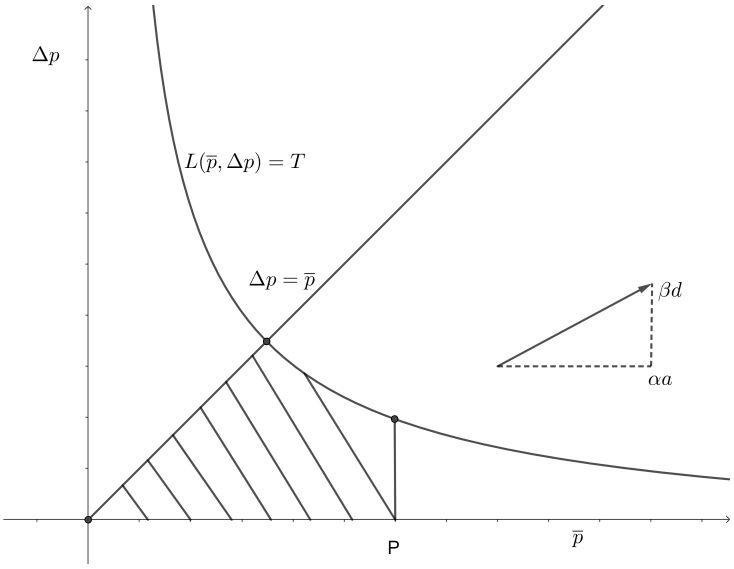

Figure 7: Feasible region of the optimization problem (8)

Now, we can substitute the optimal solution in the revenue function and ask how to choose the parameters α, a, β, d as a function of T. We obtain

$$(\alpha M_C + \beta M_F)T = (\alpha a\bar{p} + \beta d\Delta p + \alpha a + \beta e)T = (\alpha a + \beta e)T + \begin{cases} \alpha a P T + \frac{\beta d}{P^{\lambda/\kappa}} T^{1-1/\kappa}, & \alpha a > \beta d, \\ (\alpha a + \beta d) T^{1-1/(\kappa+\lambda)}, & \alpha a \leq \beta d. \end{cases}$$

As we see, for $\alpha a \leq \beta d$ the revenue is an increasing function of T whenever $\kappa + \lambda > 1$. Similarly, for $\alpha a > \beta d$ the condition $\kappa \geq 1$ ensures that the revenue is an increasing function of T.

As an extension of this simple model, it makes sense to consider a game with the customers that have a decreasing income with increasing prices. One possible revenue model for customers is

$$(A - \alpha_c M_C - \beta_c M_F)T.$$

If we move to the data-fitted lifetime function from Section 2 given by

$$L(\bar{p}, \Delta p) = \frac{1}{\Delta p^7 \left(4\sqrt{\bar{p}} - 3\frac{\Delta p}{\sqrt{\bar{p}}}\right)}, \tag{13}$$

then the feasible set is the same as in Figure 7 up to a slight redefinition of the constraint $L(\bar{p}, \Delta p) = T$. Using the same geometric argument as before, we obtain the following solution to (8) when L is given by (13):

- If $\alpha a \geq \beta d$, then the optimal solution is the right point $\bar{p} = P$, $L(\bar{p}, \Delta p) = T$ in Figure 7, which implies Δp solves the equation $3\Delta p^8 + 4P\Delta p^7 - \sqrt{P} = 0$.
- If $\alpha a < \beta d$, then the optimal solution is the left point $\bar{p} = \delta p$, $L(\bar{p}, \Delta p) = T$ in Figure 7, which implies $\bar{p} = \Delta p = \frac{1}{T^{1/7.5}}$.

The model (8) can be extended into several directions. For example, we can consider requirements to satisfy demands for capacity and flexibility. This leads to the constraints $\bar{p} \geq \underline{p}$, $\Delta p \geq \underline{\Delta p}$ by the linear dependence (9), (10). Adding the new constraints to the problem 8, the feasible region changes as depicted in Figure 8. From this, we see that for some configurations it is impossible to provide minimum capacity and flexibility and simultaneously use the pipe for T years. A possible solution is to decrease T, which is equivalent to moving the curve $L(\bar{p}, \Delta p) = T$ towards the top right.

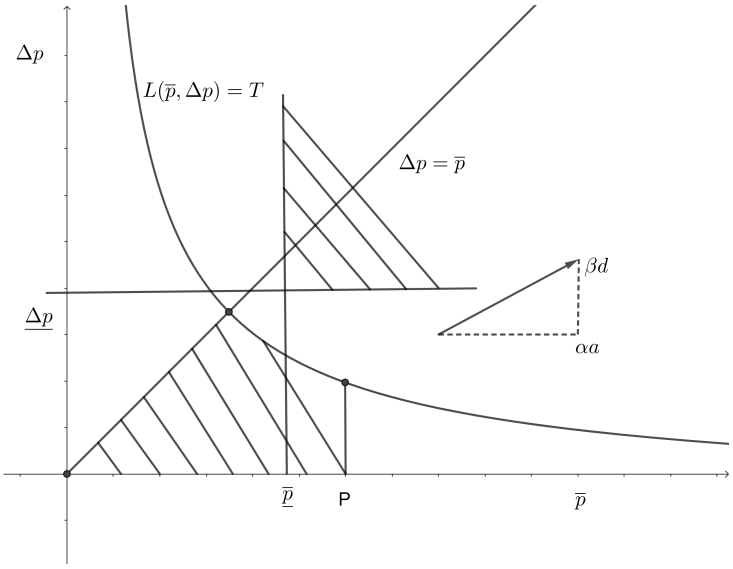

Figure 8: Feasible region of the optimization problem (8) with additional constraints

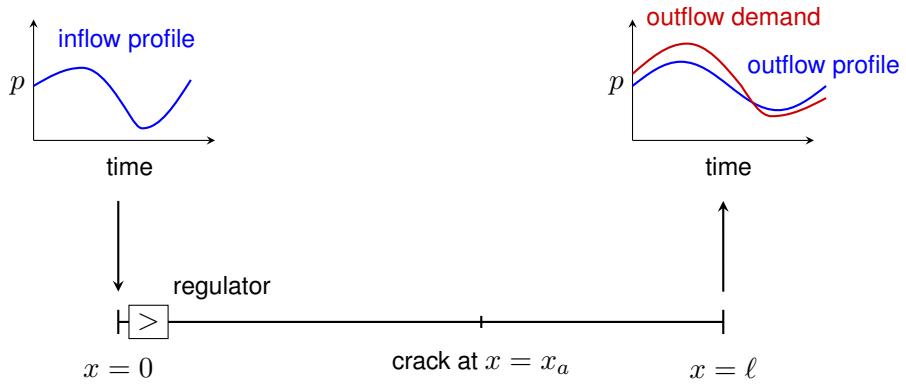

Figure 9: Pipe model for a single pipe equipped with a regulator at the inflow that is capable of reducing the inflow pressure.

3.2 Towards pricing of embrittlement based on digital twins

As the simple economic model might not be sufficiently accurate in all scenarios, we propose and discuss the following digital twin approach. Again, we focus on a single pipe modelled in one spatial dimension, this time with a regulator at the inflow point. We assume that this regulator is capable of reducing the inflow pressure, but not able to increase it. At the outlet of the pipe, we assume that a customer is expecting a hydrogen mass flow profile q_{d}. We assume that the pipe has a crack with depth $a \geq 0$ at the point x_a and depict the scenario in Figure 9. Note that extending the model to include multiple cracks is possible by making the crack depth a vector-valued, where each entry of a denotes the crack depth of a different crack of the pipe.

To accurately model the gas flow in the pipe, we consider a dynamic point of view. We consider the Euler equations

$$\begin{aligned} \partial_t \rho + \partial_x(\rho v) &= 0, \\ \partial_t(\rho v) + \partial_x(p + \rho v^2) &= -\frac{\lambda}{2D}\rho v|v|, \end{aligned} \tag{14}$$

together with the constitutive law

$$p = R_{\mathrm{s}}\, \rho\, \Theta\, z(\rho, \Theta). \tag{15}$$

Here, D and $A = \pi D^2/4$ denote the pipe diameter and the cross-sectional area of the pipe, respectively. The functions ρ, v, p and $q = A\rho v$ describe the density, velocity, pressure, and the mass flow of the gas. Moreover, R_{s} denotes the specific gas constant, λ is the friction factor of the pipe's inner wall, $z(\rho, \Theta)$ is the compression

factor and Θ is the temperature. See [DHL$^+$21] for further details on gas network modeling. In order to have a well-defined problem one further needs to specify boundary and initial conditions. We specify pressure on the inflow and mass flow on the outflow boundary (each with the option to deviate) and assume that these are such that (14) admits a solution on the time interval $[0, T]$, $T > 0$. Other approaches are possible, see for example [DKL21] and the comments therein.

To derive a pricing scheme, we take the view point of an optimal control problem. Let $u(t) \in [0, \infty)$ be the control achieved by a regulator on the inflow end of the pipe and $w(t)$ be a deviation from the expected outflow mass flow profile. Assume that the depth of the crack a is determined by an operator G which is provided as a discrete iterative scheme on a time-grid defined in Section 2.2.2. In other words, for a given pressure evolution $p(\cdot, x_a)$ and initial crack depth a_0, the function G provides the numerical solution of an ordinary differential equation describing the evolution of the crack depth over time. The functions p_{in} and q_{d} denote an external inflow pressure profile and a desired outflow mass flow profile, respectively. We arrive at the problem

$$\left.\begin{aligned} &\min_{u,w} \ \eta \int_0^T \|a\|^2 \,\mathrm{d}t + \gamma_u \int_0^T \|u\|^2 \,\mathrm{d}t + \gamma_w \int_0^T \|w\|^2 \,\mathrm{d}t \\ &\qquad\qquad \text{subject to} \\ &\qquad\qquad \text{the Euler equations (14),(15)} \\ &\qquad\qquad a = G(p(\cdot, x_a), a_0) \\ &\qquad\qquad p(t,0) = p_{\text{in}}(t) - u(t) \\ &\qquad\qquad q(t,\ell) = q_{\text{d}}(t) + w(t) \\ &\qquad\qquad u(t),\ p(t),\ q(t) \geq 0 \\ &a(0) = a_0,\ p(0,x) = p_0,\ q(0,x) = q_0. \end{aligned}\right\} \qquad \text{(OCP)}$$

Given a maximum crack depth, the optimal control problem (OCP) can be used to evaluate the life time of the gas pipe given the inflow and demand scenarios p_{in} and q_{d}. This information can then be used to find reasonable prices for the products of capacity and flexibility, as these prices are related to η, γ_u and γ_w. Here, the weighting parameters η, γ_u and γ_w can be seen as abstract prices. As noted previously, for the Euler equations we work with the inflow boundary condition $p(t, 0)$ and the outflow boundary condition $q(t, l)$ as these fit the problem description and are suitable boundary conditions for the Euler equations. For a given pressure profile p_{in} at $x = 0$, we denote by $u(t)$ the control achieved by the regulator, which can only decrease pressure (hence the sign and the non-negativity constraint on $u(t)$). On the other end of the pipe $w(t)$ quantifies the deviation from the expected mass flow profile $q_d(t)$. As pressure and mass flow should be non-negative to be physically feasible we include the corresponding constraints as well. For any time $t \in [0, T]$ and point $x \in [0, \ell]$ the Euler equations then determine the state $(p, q)(t, x)$. The cost functional penalizes high crack depths a as well as large deviations u, w.

We suggest to use a direct approach to solve the problem (OCP). State-of-the-art are the following methods [HS24]:

- Sequential quadratic programming can be applied to (adaptive) implicit box schemes, where gradients are computed using a discrete adjoint approach [DKL21];
- Interior-point methods can be applied to pseudospectral collocation methods, where gradients then come in sparse form [ZCB15].
- The structure of Euler discretizations can also be exploited in tailored primal-dual interior-point solvers [Ste07];
- Gradient information for certain discretizations can also be obtained from formal adjoint approaches [HS20, HS07].

Note that the constraint $a = G(p, a_0)$ is already provided as an iterative discrete time scheme. Hence, only the time-grid for the discretization of the Euler equation and this scheme have to be aligned and to be included in the adjoint computations. The use of direct methods in principle also allows extensions of the problem (OCP) to small to medium sized networks. The resources above also cover simulation techniques for gas transport on a network.

4 Conclusion

Addressing hydrogen embrittlement is crucial for the successful integration of hydrogen technologies in Germany. This involves a comprehensive understanding of the mechanisms behind hydrogen embrittlement and its impact on the lifespan of pipeline infrastructure.

In this article, we discussed the modelling of hydrogen embrittlement and pricing strategies to mitigate lifetime shortening effects during operation. On one hand, we observed that currently used embrittlement models such as Paris' law may fail to adequately capture critical processes occurring in hydrogen networks, and suggested an continuum model as an alternative approach. On the other hand, to allow for simplified pipe-lifetime considerations, we formulated a lifetime function based on a cycling loading assumption. Subsequently, using this simplified lifetime function and based around the concepts of capacity and flexibility, we formulated a pricing model aimed to capture the effects of pipe embrittlement on the operation span of a single gas pipe. Finally, we suggested techniques to set-up a digital twin model for estimating pipe lifetimes with possibly more complex crack growth observations.

Possible topics for future work are to study parameter fitting of Paris' law using continuum based models for improving their predictive power, to further develop the proposed digital twin model, and to compare the solutions of the proposed approaches. Moreover, models and coupling effects related to hydrogen embrittlement remain a subject of ongoing debate. Therefore, fundamental contributions to the modeling of fatigue, crack growth, plasticity, and dislocation dynamics in the presence of hydrogen diffusion could significantly advance the field.

Acknowledgment This article reports research initiated within the 175th European Study Group with Industry at the Weierstrass Institute for Applied Analysis and Stochastics in Berlin, September 18-22, 2023. We acknowledge the discussions and the financial support from the involved industry partner Open Grid Europe GmbH. Moreover, we acknowledge the discussions and contributions by Tobias Breiten, Timo Kreimeier, and Barnum Swannell to the results here reported. Further, F.M. Hante and A. Karsai thank the Deutsche Forschungsgemeinschaft (DFG) for their support within the subprojects A03 and B03 in the Sonderforschungsbereich/Transregio 154 *Mathematical Modelling, Simulation and Optimization using the Example of Gas Networks* (Project 239904186). Z. Amer und P. Farrell thank the Leibniz competition 2020 (NUMSEMIC, J89/2019). D. Peschka acknowledges funding by DFG within the SPP 2171 *Dynamic Wetting of Flexible, Adaptive, and Switchable Surfaces* (Project 422792530).

References

[AWL+18] R. L. Amaro, R. M. White, C. P. Looney, E. S. Drexler, and A. J. Slifka. Development of a model for hydrogen-assisted fatigue crack growth of pipeline steel. *Journal of Pressure Vessel Technology*, 140(2):021403, 2018.

[Bun20] Bundesministerium für Wirtschaft und Klimaschutz. Die Nationale Wasserstoffstrategie. `https://www.bmwk.de/Redaktion/DE/Publikationen/Energie/die-nationale-wasserstoffstrategie.html`, 2020.

[CMMP22] C. Cui, R. Ma, and E. Martínez-Pañeda. A generalised, multi-phase-field theory for dissolution-driven stress corrosion cracking and hydrogen embrittlement. *Journal of the Mechanics and Physics of Solids*, 166:104951, 2022.

[DB76] N. E. Dowling and J. A. Begley. Fatigue crack growth during gross plasticity and the j-integral. 1976.

[DHL+21] P. Domschke, B. Hiller, J. Lang, V. Mehrmann, R. Morandin, and C. Tischendorf. Gas network modeling: An overview. *Preprint*, page 53, 2021.

[DKL21] P. Domschke, O. Kolb, and J. Lang. Fast and reliable transient simulation and continuous optimization of large-scale gas networks. *Mathematical Methods of Operations Research*, 2021.

[DS82] S. D. Downing and D. F. Socie. Simple rainflow counting algorithms. *International Journal of Fatigue*, 4(1):31–40, 1982.

[FKE67] R. G. Forman, V. E. Kearney, and R. M. Engle. Numerical analysis of crack propagation in cyclic-loaded structures. 1967.

[HG20] C. Huang and X. Gao. Phase field modeling of hydrogen embrittlement. *International Journal of Hydrogen Energy*, 45(38):20053–20068, 2020.

[HLM+17] F. M. Hante, G. Leugering, A. Martin, L. Schewe, and M. Schmidt. Challenges in optimal control problems for gas and fluid flow in networks of pipes and canals: From modeling to industrial applications. *Industrial mathematics and complex systems: Emerging mathematical models, methods and algorithms*, pages 77–122, 2017.

[HS07] M. Herty and V. Sachers. Adjoint calculus for optimization of gas networks. *Networks and Heterogeneous Media*, 2(4):733–750, 2007.

[HS20] M. Hintermüller and N. Strogies. Identification of the friction function in a semilinear system for gas transport through a network. *Optimization Methods and Software*, 35(3):576–617, 2020.

[HS23] F. M. Hante and M. Schmidt. Gas transport network optimization: mixed-integer nonlinear models. In *Encyclopedia of Optimization*, pages 1–8. Springer, 2023.

[HS24] F. M. Hante and M. Schmidt. Gas transport network optimization: PDE-constrained models. In *Encyclopedia of Optimization*. Springer Nature, 3 edition, 2024.

[KHPS15] T. Koch, B Hiller, M. E. Pfetsch, and L. Schewe. *Evaluating gas network capacities*. SIAM, 2015.

[KP23] M. A. Kappes and T. Perez. Hydrogen blending in existing natural gas transmission pipelines: a review of hydrogen embrittlement, governing codes, and life prediction methods. *Corrosion Reviews*, 41(3):319–347, 2023.

[LDC+22] A. Laureys, R. Depraetere, M. Cauwels, T. Depover, S. Hertelé, and K. Verbeken. Use of existing steel pipeline infrastructure for gaseous hydrogen storage and transport: A review of factors affecting hydrogen induced degradation. *Journal of Natural Gas Science and Engineering*, 101:104534, 2022.

[LMZ+20] X. Li, X. Ma, J. Zhang, E. Akiyama, Y. Wang, and X. Song. Review of hydrogen embrittlement in metals: hydrogen diffusion, hydrogen characterization, hydrogen embrittlement mechanism and prevention. *Acta Metallurgica Sinica (English Letters)*, 33:759–773, 2020.

[MHW10] C. Miehe, M. Hofacker, and F. Welschinger. A phase field model for rate-independent crack propagation: Robust algorithmic implementation based on operator splits. *Computer Methods in Applied Mechanics and Engineering*, 199(45-48):2765–2778, 2010.

[MWH10] C. Miehe, F. Welschinger, and M. Hofacker. Thermodynamically consistent phase-field models of fracture: Variational principles and multi-field fe implementations. *International journal for numerical methods in engineering*, 83(10):1273–1311, 2010.

[NBTB23] D. H. Najafabadi, A. Barabi, D. Thibault, and M. Brochu. Hydrogen-enhanced fatigue crack growth of martensitic stainless steel: A predictive model and experimental validation. *Theoretical and Applied Fracture Mechanics*, page 104066, 2023.

[NJ98] J. C. Newman Jr. The merging of fatigue and fracture mechanics concepts: a historical perspective. *Progress in Aerospace Sciences*, 34(5-6):347–390, 1998.

[NJR81] J. C. Newman Jr. and I. S. Raju. An empirical stress-intensity factor equation for the surface crack. *Engineering Fracture Mechanics*, 15(1-2):185–192, 1981.

[OFM25] H. Oesterlin, C. Fischer, and T. Michler. Evaluation of lifetime predictions for future hydrogen pipelines by different fracture mechanics-based design codes. *Energy Technology*, 13(2):2301012, 2025.

[OMN85] K. Ogura, Y. Miyoshi, and I. Nishikawa. Fatigue crack growth and closure of small cracks at the notch root. *Current research on fatigue cracks(A 86-33002 14-39). Kyoto, Society of Materials Science, 1985,*, pages 57–78, 1985.

[PCCC06] N. Pugno, M. Ciavarella, P. Cornetti, and A. Carpinteri. A generalized paris' law for fatigue crack growth. *Journal of the Mechanics and Physics of Solids*, 54(7):1333–1349, 2006.

[PE63] P. Paris and F. Erdogan. A critical analysis of crack propagation laws. *Journal of Basic Engineering*, 85(4):528–533, 12 1963.

[PZB+19] L. B. Peral, A. Zafra, S. Blasón, C. Rodríguez, and J. Belzunce. Effect of hydrogen on the fatigue crack growth rate of quenched and tempered crmo and crmov steels. *International Journal of Fatigue*, 120:201–214, 2019.

[SGAPJ21] D. Sandana, N. Gallon, R. Andrews, and R. Palmer-Jones. Crack management of hydrogen pipelines. 2021.

[SMS23] M. Steiner, U. Marewski, and H. Silcher. Report: H2-Tauglichkeit von Stählen. Technical report, Deutscher Verein des Gas- und Wasserfaches (DVGW), 2023. https://www.dvgw.de/themen/forschung-und-innovation/forschungsprojekte/dvgw-forschungsprojekt-h2-tauglichkeit-von-staehlen.

[Ste07] M. C. Steinbach. On PDE solution in transient optimization of gas networks. *Journal of Computational and Applied Mathematics*, 203(2):345–361, 2007.

[TBW20] M. Thomas, C. Bilgen, and K. Weinberg. Analysis and simulations for a phase-field fracture model at finite strains based on modified invariants, 2020.

[Tom68] B. Tomkins. Fatigue crack propagation—an analysis. *Philosophical magazine*, 18(155):1041–1066, 1968.

[VCS12] L. Vergani, C. Colombo, and A. Sciuccati. Influence of hydrogen environment on crack growth rate. *Gruppo Italiano di frattura*, pages 635–642, 2012.

[Wal70] K. Walker. The effect of stress ratio during crack propagation and fatigue for 2024-t3 and 7075-t6 aluminum. 1970.

[WDM+19] D. Wan, Y. Deng, J. I. H. Meling, A. Alvaro, and A. Barnoush. Hydrogen-enhanced fatigue crack growth in a single-edge notched tensile specimen under in-situ hydrogen charging inside an environmental scanning electron microscope. *Acta Materialia*, 170:87–99, 2019.

[Wol70] E. Wolf. Fatigue crack closure under cyclic tension. *Engineering fracture mechanics*, 2(1):37–45, 1970.

[YM17] T. Yoshimoto and T. Matsuo. An investigation into the frequency dependence upon the fatigue crack growth rate conducted by a novel fatigue testing method with in-situ hydrogen-charging. In *Journal of Physics: Conference Series*, volume 843, page 012050. IOP Publishing, 2017.

[YSM22] S. Yan, C. Schreiber, and R. Müller. An efficient implementation of a phase field model for fatigue crack growth. *International Journal of Fracture*, 237(1-2):47–60, 2022.

[ZÁB+23] A. Zafra, G. Álvarez, G. Benoit, G. Henaff, E. Martínez-Paneda, C. Rodríguez, and J. Belzunce. Hydrogen-assisted fatigue crack growth: pre-charging vs in-situ testing in gaseous environments. *Materials Science and Engineering: A*, 871:144885, 2023.

[ZCB15] A. Zlotnik, M. Chertkov, and S. Backhaus. Optimal control of transient flow in natural gas networks. In *2015 54th IEEE Conference on Decision and Control (CDC)*, pages 4563–4570, 2015.

A Appendix

A.1 Documentation of the full mathematical model

Consider a pipe of length w, thickness t_*, and center-diameter D_a, see Figure 1. The centre diameter is defined as the inner diameter plus the wall's thickness. Furthermore, consider an axial crack with depth a and half-length c. The evolution under cycling of both a and c can be described using the difference equation:

$$\frac{\mathrm{d}X}{\mathrm{d}N} = \begin{cases} 4.4 \cdot 10^{-13}(1+3R)\Delta K_X^7 \sqrt{p_{\mathrm{H}_2}} & \text{if } \Delta K_a \le K_{\text{crit}} \\ 1.2 \cdot 10^{-7}(1+3R)\Delta K_X^3 & \text{otherwise} \end{cases}, \tag{16}$$

where we use X as a placeholder for both a or c, i.e. $X \in \{a, c\}$. Additionally, N is the number of cycles, R is the stress ratio, ΔK_X is the stress intensity range, p_{H_2} is hydrogen's partial gas pressure in bar, and $K_{\text{crit}} = \left(3.6667 \cdot 10^{-6}\sqrt{p_{\mathrm{H}_2}}\right)^{-0.25}$ MPa m$^{1/2}$ is the empirically derived critical stress intensity factor [SMS23]. The stress ratio R and the stress intensity range ΔK_X are defined

$$R = \frac{p_{\min}}{p_{\max}} = \frac{\bar{p} - \Delta p}{\bar{p}}, \qquad \Delta K_X = M f_w M_{mX} (\Delta\sigma + \Delta p)\sqrt{\frac{a\pi}{1000}},$$

with the minimal and maximal pressure during a cycle being $p_{\min}$ and $p_{\max}$. All lengths are in mm. The variables contained in this definition are given as follows:

$$\Delta\sigma = \frac{\Delta p \cdot D_a}{2t_*}, \qquad k = \frac{a}{2c},$$

$$\lambda = \frac{1.818c}{\sqrt{t_*\left(\frac{D_a}{2} - t_*\right)}}, \qquad M_t = \sqrt{\frac{1.02 + 0.4411\lambda^2 + 0.006124\lambda^4}{1 + 0.02642\lambda^2 + 1.533 \cdot 10^{-6}\lambda^4}},$$

$$M = \frac{1 - 0.85\frac{a}{M_t t_*}}{1 - 0.85\frac{a}{t_*}}, \qquad f_w = \left(\cos\left(\pi\frac{c}{w}\sqrt{\frac{a}{t_*}}\right)\right)^{-1/2},$$

$$f_{\theta,a} = \begin{cases} 1 & 0 \le k < 0.5 \\ \sqrt{\frac{c}{a}} & 0.5 \le k \le 1 \end{cases}, \qquad g_c = \begin{cases} 1.1 + 0.35\left(\frac{a}{t_*}\right)^2 & 0 \le k < 0.5 \\ 1.1 + 0.35\frac{c}{a}\left(\frac{a}{t_*}\right)^2 & 0.5 \le k \le 1 \end{cases},$$

$$g_a = 1, \qquad \Phi = \begin{cases} \sqrt{1 + 1.464(a/c)^{1.65}} & 0 \le k < 0.5 \\ \sqrt{1 + 1.464(c/a)^{1.65}} & 0.5 \le k \le 1 \end{cases},$$

$$f_{\theta,c} = \begin{cases} \sqrt{\frac{a}{c}} & 0 \le k < 0.5 \\ 1 & 0.5 \le k \le 1 \end{cases}, \qquad M_{mX} = \left(M_1 + M_2\left(\frac{a}{t_*}\right)^2 + M_3\left(\frac{a}{t_*}\right)^4\right)\frac{g_X f_{\theta,X}}{\Phi},$$

$$M_1 = \begin{cases} 1.13 - 0.09\frac{a}{c} & 0 \le k < 0.5 \\ \sqrt{\frac{c}{a}}\left(1 + 0.04\frac{c}{a}\right) & 0.5 \le k \le 1 \end{cases}, \qquad M_2 = \begin{cases} \frac{0.89}{0.2 + a/c} - 0.54 & 0 \le k < 0.5 \\ 0.2\left(\frac{c}{a}\right)^4 & 0.5 \le k \le 1 \end{cases},$$

$$M_3 = \begin{cases} 0.5 - \frac{1}{0.65 + a/c} + 14(1 - a/c)^{24} & 0 \le k < 0.5 \\ -0.11\left(\frac{c}{a}\right)^4 & 0.5 \le k \le 1 \end{cases}.$$

With the definitions above, the function $f(a)$ in (5) is of the form

$$f(a) = 4.4 \cdot 10^{-13}\left(\frac{\Delta K_a}{\Delta p}\right)^7 \quad \text{where} \quad \frac{\Delta K_a}{\Delta p} = M f_w M_{ma}\sqrt{\frac{a\pi}{1000}}\left(1 + \frac{D_a}{2t_*}\right). \tag{17a}$$

Note that above we assume that the crack length $c = c_0$ does not evolve substantially from its initial value and that mainly the crack depth a contributes to the lifetime function. For pure hydrogen we used $(p_{\mathrm{H}_2}/\bar{p})^{1/2} = 1$ such that

$$g(\Delta p, \bar{p}) = \left(4 - 3\frac{\Delta p}{\bar{p}}\right)(\Delta p)^7\sqrt{\bar{p}} \quad \text{and thus} \quad \frac{\mathrm{d}a}{\mathrm{d}N} = g(\Delta p, \bar{p}) f(a). \tag{17b}$$